

# Superparamagnetic Iron Oxide Nanoparticles Conjugated with A $\beta$ Oligomer-Specific scFv Antibody and Class A Scavenger Receptor Activator Show Therapeutic Potentials for Alzheimer's Disease

**Xiao-ge Liu**

Institute of Process Engineering Chinese Academy of Sciences

**Lun Zhang**

Institute of Process Engineering Chinese Academy of Sciences

**Shuai Lu**

Institute of Process Engineering Chinese Academy of Sciences

**Dong-qun Liu**

Institute of Process Engineering Chinese Academy of Sciences

**Ya-ru Huang**

Institute of Process Engineering Chinese Academy of Sciences

**Jie Zhu**

Institute of Process Engineering Chinese Academy of Sciences

**Wei-wei Zhou**

Institute of Process Engineering Chinese Academy of Sciences

**Xiao-lin Yu**

Institute of Process Engineering Chinese Academy of Sciences

**Rui-tian Liu** (✉ [rtliu@ipe.ac.cn](mailto:rtliu@ipe.ac.cn))

Institute of Process Engineering Chinese Academy of Sciences <https://orcid.org/0000-0002-4297-4765>

---

## Research

**Keywords:** Alzheimer's disease,  $\beta$ -amyloid, oligomer, class A scavenger receptor, Therapy

**Posted Date:** June 30th, 2020

**DOI:** <https://doi.org/10.21203/rs.3.rs-38153/v1>

**License:**   This work is licensed under a Creative Commons Attribution 4.0 International License.

[Read Full License](#)

**Version of Record:** A version of this preprint was published on November 7th, 2020. See the published version at <https://doi.org/10.1186/s12951-020-00723-1>.

# Abstract

**Background:** Alzheimer's disease (AD) is an incurable and progressive neurodegenerative disorder. Disease-modifying strategies to prevent or delay AD progression are urgently needed. A $\beta$  oligomers (A $\beta$ O), rather than monomers or fibrils, are considered as the most neurotoxic species. Therapeutic approaches that direct against these oligomers and promote A $\beta$  clearance may have great value for AD intervention.

**Results:** We here reported the novel multifunctional nanoparticle W20/XD4-SPIONs, which were constructed by conjugating oligomer-specific scFv antibody W20 and class A scavenger receptor activator XD4 onto superparamagnetic iron oxide nanoparticles (SPIONs). Besides the diagnostic value, W20/XD4-SPIONs retained the properties of W20 and XD4 by inhibiting A $\beta$  aggregation, attenuating A $\beta$ O-induced cytotoxicity and increasing microglial phagocytosis of A $\beta$ . When applied to AD transgenic mouse model, W20/XD4-SPIONs significantly rescued cognitive deficits and alleviated neuropathology of AD transgenic mice.

**Conclusion:** These results suggest that W20/XD4-SPIONs are a promising therapeutic agent for AD. As a molecular probe, W20/XD4-SPIONs also specifically and sensitively bind to the A $\beta$ O in AD brains to provide an MRI signal, demonstrating that W20/XD4-SPIONs are a promising agent for early-stage AD.

## Background

Alzheimer's disease (AD) is the most common neurodegenerative disorder, which is characterized by progressive memory loss and cognitive decline. The pathological hallmarks of AD are the presence of extracellular  $\beta$ -amyloid (A $\beta$ ) plaques and intraneuronal neurofibrillary tangles aggregated from the microtubule-associated protein tau[1]. The prevalence of AD is increasing, which causes heavily social and economic burden over the world. Despite decades of efforts to understand the pathophysiology and to develop therapies for AD, effective strategies to prevent and cure it remain elusive[2]. The amyloid cascade hypothesis suggests that A $\beta$  oligomers (A $\beta$ O), rather than monomers or insoluble fibrils, are the primary toxic species in the pathogenesis of AD [3]. A $\beta$ O appear in the brains of AD patients decades before the onset of clinical symptoms[4–6], suggesting their potential use as a more appealing target than plaques at the early stage of AD. Moreover, mounting of evidences support a pivotal role of A $\beta$ O in neuronal dysfunction and synapse loss in AD [7–9]. A $\beta$ O bind to the plasma membranes of neuronal cells, trigger transmembrane signaling and abnormal intracellular changes, which lead to synapse failure and ultimately cognitive impairment[10]. Therefore, targeting to A $\beta$ O will be attractive therapeutic strategy for AD.

Many clinical trials showed that the effector fragment of antibodies induced remarkable side effects[11–13]. In previous studies, we reported that an oligomer specific single-chain variable fragment antibody W20, which bound to toxic A $\beta$ O and inhibited their neurotoxicity with higher safety [14–16]. However, W20 showed low efficiency in A $\beta$ O clearance. A heptapeptide XD4 can resolve such problem. XD4

peptide was isolated from a Ph.D.-C7C library by phage display, which can activate the class A scavenger receptor (SR-A) on the microglia and promotes the phagocytosis of A $\beta$ O $_s$  [17]. Therefore, we conjugated antibody W20 and SR-A activator XD4 onto superparamagnetic iron oxide nanoparticles (SPIONs) to construct a novel kind of multifunctional nanoparticle W20/XD4-SPIONs. In previous studies, we demonstrated that W20/XD4-SPIONs, as an A $\beta$ O $_s$ -targeted molecular MRI contrast probe, exhibited early diagnostic potentials for AD[18]. Moreover, W20/XD4-SPIONs showed the properties of good biocompatibility, high stability and low cytotoxicity. Here, we investigated whether W20/XD4-SPIONs retained the dual anti-A $\beta$  functions of W20 and XD4 *in vitro*, and assessed its effects on cognitive performance and neuropathology in the APP/PS1 transgenic mouse model.

## Results

### **W20/XD4-SPIONs inhibited A $\beta$ aggregation and cytotoxicity and reduced the inflammatory cytokine production *in vitro***

In our previous studies, oligomer-specific antibody W20 and SR-A activator XD4 have been shown to inhibit A $\beta$  aggregation, attenuate A $\beta$ O $_s$ -induced cytotoxicity and reduce the production of proinflammatory cytokines[14, 16, 17]. Here we investigated whether the conjugation of W20 and XD4 onto SPIONs (W20/XD4-SPIONs, Fig. 1a) retained their anti-A $\beta$  functions. In A $\beta$  aggregation assay, A $\beta$  alone showed the expected nucleation-dependent polymerization process, while both W20/XD4-SPIONs and W20-SPIONs significantly inhibited A $\beta$  aggregation in a concentration-dependent manner with complete suppression at 1000  $\mu$ g/mL (Fig. 1b). Similarly, in MTT assay, A $\beta$ O $_s$  alone or combined with unconjugated-SPIONs caused a significant reduction in cell viability, while W20/XD4-SPIONs and W20-SPIONs inhibited A $\beta$ O $_s$ -induced cytotoxicity by 51.1% and 49.3%, respectively (Fig. 1c). Moreover, A $\beta$ O $_s$  promoted inflammatory cytokine production in BV-2 cells, such as IL-6 and TNF- $\alpha$ , whereas both W20/XD4-SPIONs and W20-SPIONs significantly reduced the levels of IL-6 and TNF- $\alpha$  in the cell supernatants (Fig. 1d, e). We further determined the levels of inflammatory mediators such as iNOS and COX-2 in BV-2 cell lysates by western-blot (Fig. 1f). The results demonstrated that the levels of iNOS and COX-2 were all elevated after A $\beta$ O $_s$  challenge but significantly decreased by W20/XD4-SPIONs or W20-SPIONs treatment (Fig. 1g).

### **W20/XD4-SPIONs rescued cognitive deficits in AD mice**

After 28 days treatment of W20/XD4-SPIONs, we applied object recognition test, Y-maze test and Morris water maze (MWM) test to assess the effects of the serial of SPIONs on the cognitive performance of AD mice (Fig. 2a). In object recognition test, vehicle- or unconjugated SPIONs-treated AD mice did not show any preference to the novel object, while AD mice treated with W20/XD4-SPIONs or W20-SPIONs exhibited a remarkable increase in investigation to the novel object (Fig. 2b). In Y-maze test, WT mice spent more time in the novel arm, whereas vehicle- or unconjugated SPIONs-treated AD mice had no preference for the novel arm (Fig. 2c, d). In comparison, AD mice treated with W20 and/or XD4 conjugated-SPIONs

showed significantly improved spatial memory by more residence time (Fig. 2c) and more entries (Fig. 2d) in the novel arm. Notably, W20/XD4-SPIONs showed the best effect on the memory retention in all tested groups. Consistently, in MWM test, AD mice treated with W20/XD4-SPIONs or W20-SPIONs took shorter time to reach the platform than vehicle-treated AD mouse controls during the acquisition period (Fig. 2e). In the probe trials, AD mice treated with W20/XD4-SPIONs or W20-SPIONs also exhibited spatially-oriented swimming behavior, shorter escape latencies (Fig.2f), more times of platform crossing (Fig. 2g) and more time spent in the target quadrant (Fig. 2h) than vehicle-treated or unconjugated SPIONs-treated AD mice. Moreover, no significant difference in the swimming speed of mice was observed within the mouse groups in the training period and the probe trials of MWM test, indicating that neither group was impaired in motility and exploratory activities. Collectively, these findings suggested that W20/XD4-SPIONs and W20-SPIONs significantly attenuated cognitive deficits in AD mice, and W20/XD4-SPIONs exhibited better effects on the cognition and memory of AD mice than W20-SPIONs did.

## **W20/XD4-SPIONs reduced neuroinflammation in the brains of AD mice**

The increased glial activation and inflammatory cytokine production result in neuroinflammation, which are strongly associated with AD onset and progression. We evaluated the gliosis in the brains of AD mice and their WT littermates by GFAP immunostaining (Fig. 3a) and Iba-1 immunostaining (Fig. 3b). The results showed that W20/XD4-SPIONs significantly reduced astrocytosis (Fig. 3c) and microgliosis (Fig. 3d) in the brains of AD mice as compared with the vehicle treatment.

To further assess the effects of the serial of SPIONs on the inflammatory cytokine production, we determined the levels of IL-1 $\beta$ , IL-6 and TNF- $\alpha$  in the mouse brain lysates by ELISA assay. Compared with the vehicle-treated AD mouse controls, W20/XD4-SPIONs resulted in a significant decrease in the levels of IL-1 $\beta$  by 41.7% (Fig. 3e), IL-6 by 50.1% (Fig. 3f), and TNF- $\alpha$  by 55.6% (Fig. 3g), respectively.

## **W20/XD4-SPIONs increased GSH level and reduced ROS level in the brains of AD mice**

Toxic A $\beta$ Os lead to extensive oxidative stress in neuronal cells, which play a key role in AD pathogenesis. GSH/GSSG ratio is considered as an ideal indicator for the oxidative stress level. We determined the levels of GSH, GSSG and ROS in the brain lysates of AD mice and their WT littermates treated with various SPIONs. The results showed that both W20/XD4-SPIONs and W20-SPIONs significantly increased GSH levels (Fig. 3h), decreased GSSG levels (Fig. 3i) and increased GSH/GSSG ratios (Fig. 3j) in AD mice, as compared with the vehicle-treated controls. A significant decrease in ROS level was also observed in the brains of AD mice treated with W20/XD4-SPIONs (Fig. 3k).

## **W20/XD4-SPIONs reduced A $\beta$ burden in the brains of AD mice**

We next evaluated A $\beta$  burden in the brains of AD mice treated with the serial of SPIONs. A $\beta$  plaques in the mouse brains were detected by 6E10 immunostaining. Compared with the vehicle treatment, W20 and/or XD4 conjugated-SPIONs significantly reduced the plaque areas in the brains of AD mice, and W20/XD4-SPIONs treatment resulted in the lowest plaque burdens (Fig. 4a, b). The levels of soluble and insoluble A $\beta$  in the mouse brain lysates were further determined by ELISA. All conjugated-SPIONs, including W20-, XD4- and W20/XD4-SPIONs significantly reduced the levels of insoluble A $\beta$ 40 and A $\beta$ 42 (Fig. 4c, d) in AD brains. W20/XD4-SPIONs also significantly reduced soluble A $\beta$ 42 levels in the brains of AD mice (Fig. 4f), while soluble A $\beta$ 40 levels didn't reach the statistical difference by various SPIONs treatment (Fig. 4e).

## **W20/XD4-SPIONs rescued synapse loss in the brains of AD mice**

The synaptic dysfunction and synapse loss correlate positively with cognitive decline in AD. A $\beta$ Os can impair synapse structure and function and lead to the decrease of synapse number. Here we evaluated the synaptic levels in mouse brains by immunohistochemistry using anti-PSD-95 and anti-synaptophysin antibodies, respectively (Fig. 5a, b). A significant decrease in both synaptic markers of PSD-95 and synaptophysin was observed in the cortex and hippocampus of AD mice compared with WT mice, while W20/XD4-SPIONs and W20-SPIONs significantly increased the levels of PSD-95 and synaptophysin in AD brains, XD4-SPIONs only increased synaptophysin levels (Fig. 5c). These findings suggested that SPIONs conjugated with W20 and XD4 significantly rescued synapse loss in the brains of AD mice.

## **W20/XD4-SPIONs enhanced A $\beta$ Os engulfment by microglia in the brains of AD mice**

To determine whether W20/XD4-SPIONs can promote A $\beta$ Os engulfment by microglia in AD brains, the A $\beta$  puncta in the Iba-1-positive microglia of mouse brains was qualified (Fig. 6a). We observed a significant increase in the microglial phagocytosis of A $\beta$  in W20/XD4-SPIONs-treated AD mice compared with vehicle-treated AD controls. XD4-SPIONs and W20-SPIONs also resulted in a slight and significant increases in A $\beta$  engulfment by microglia, but less than W20/XD4-SPIONs did (Fig. 6b).

## **Discussion**

Lots of clinical evidences revealed that A $\beta$ Os, but not A $\beta$  monomers and fibrils correlate well with AD dementia [10, 19]. Approaches targeting A $\beta$ Os may have promising applications in AD treatment. The present work takes advantage of A $\beta$ 0-specific antibody W20 and SR-A activator XD4, when conjugated to SPIONs together, the obtained novel multifunctional nanoparticles W20/XD4-SPIONs can recognize and

promote microglial phagocytosis of toxic oligomers in the AD mouse brains. When administrated to an AD mouse model for 28 days, W20/XD4-SPIONs rescued the cognitive deficits and reduced neuropathology in AD mice, showed promising therapeutic potentials for AD upon early diagnostic value.

More than ten antibodies and vaccines targeting A $\beta$  failed in the clinical trials. Most immunotherapy caused apparent side effects such as hydrocephalus, inflammation, amyloid-related imaging abnormalities with edema (ARIA-E), and ARIA-haemosiderin (ARIA-H)[20, 21], which were partly induced by complement-dependent cytotoxicity and microglia activation. The complex of A $\beta$  and corresponding antibodies activated complement, producing proinflammatory fragments C3a and C5a. Also the resultant complement fragment such as C3b may further activate CR3 and Fc $\gamma$  receptors of microglia, exacerbating neuroinflammation[22]. Therefore, the effector fragment of antibody plays a key role in the progression of side effects. ScFv antibody W20 is A $\beta$ O-specific and without Fc fragment, which would eliminate associated adverse effects to a great extent.

However, W20 may reduce the microglial clearance of the complexes. To solve this problem, we further introduce the microglial SR-A activator XD4 in the nanoparticles. Glial phagocytosis and degradation of A $\beta$  is believed to be the key mechanisms of the initial defense of the brains against toxic A $\beta$  aggregates [23]. Multiple cell surface receptors of microglia, including SR-A[24–26], class B scavenger receptor type I (SR-BI), CD36[27], CD14, CD47 and toll-like receptors (TLRs), have been shown to mediate A $\beta$  uptake and degradation [28]. With AD progression, microglia are overactivated and lose their intrinsic beneficial function of A $\beta$  clearance, leading to A $\beta$  accumulation, increased levels of ROS and proinflammatory cytokines, neuroinflammation and neurodegeneration [29]. SR-A activation is beneficial for A $\beta$  clearance and AD treatment. Compared with the activation of CR3 and Fc $\gamma$  receptors, SR-A activation generated much less proinflammatory factors. Heptapeptide XD4 can activate SR-A on the glia by increasing the binding of A $\beta$  to SR-A without the induction of proinflammatory cytokines, thereby promoting glial phagocytosis of A $\beta$ O $s$  and inhibiting A $\beta$ O $s$ -induced cytotoxicity[17]. In present study, W20/XD4-SPIONs retained XD4 property for SR-A activation, which significantly enhanced microglial engulfment of the A $\beta$ O $s$  recognized by W20, resulting in the pronounced improvement of cognitive performance in AD mice. W20/XD4-SPIONs containing these two safe components may exhibit good safety, which was confirmed by the present *in vivo* results that W20/XD4-SPIONs did not induce any adverse effects on cognitive function and neurophysiology in WT mice after 28 days of treatment (Fig. 2–5).

In summary, besides the potential application in early diagnosis for AD, the multifunctional nanoparticles W20/XD4-SPIONs significantly rescued cognitive deficits, reduced A $\beta$  burden and attenuated neuroinflammation, oxidative stress and synapse loss in AD mice. As W20/XD4-SPIONs contain both W20 and XD4, possess dual therapeutic function, this kind of nanoparticles show the most beneficial effect on AD mice relative to W20-SPIONs or XD4-SPIONs, and exhibit promising therapeutic potentials for AD. However, the safety of W20/XD4-SPIONs should be thoroughly assessed using several kinds of animal models. Furthermore, a formal study of the pharmacokinetics of W20/XD4-SPIONs should be carried out to investigate the distribution and the half-life in brains.

## Methods

## Materials

A $\beta$ 42 and XD4 peptide was synthesized from Chinese Peptide Company (Hangzhou, China). Both A $\beta$ 40 and A $\beta$ 42 kits for A $\beta$  measurement were purchased from Immuno-Biological Laboratories Co., Ltd. (Gunma, Japan). TNF- $\alpha$ , IL-1 $\beta$  and IL-6 ELISA kits were obtained from Neobioscience Technology Co., Ltd. (Beijing, China). The following antibodies were used: 6E10 (monoclonal raised against A $\beta$ 1-16, Signet, SIG39300), W20 (oligomer-specific antibody, developed and prepared in our laboratory), anti-Iba-1 antibody (GenTex, GTX100042), anti-GFAP antibody (Abcam, ab53554), anti-PSD-95 antibody (Abcam, ab18258), anti-synaptophysin antibody (Abcam, ab32127), anti-GAPDH antibody (CST, 2118S), goat anti-rabbit secondary antibody conjugated to Alexa Fluor 488 (Santa Cruz, I1112) or Alexa Fluor 594 (Abcam, ab150084). HRP-conjugated goat anti-mouse or rabbit IgG antibody (Zhongshan Golden Bridge Biotechnology, Beijing, China).

$$\text{conjugation (\%)} = \frac{\text{total added W20 or XD4} - \text{W20 or XD4 in supernatant}}{\text{total added W20 or XD4}} \times 100$$

## Preparation of W20 and/or XD4 conjugated-SPIONs

W20 and/or XD4 conjugated-SPIONs were synthesized according to previous methods[18]. Briefly, the PEG-coated SPIONs were synthesized by a “one-pot” synthetic approach. 2.1 g of Fe(acac)<sub>3</sub>, 7.9 mL of oleylamine, and 24 g of HOOC-PEG-COOH (Mn = 2000) were dissolved in 100 mL of diphenyl ether solution and incubated at 80°C for 4 h with stirring at 400 rpm in anaerobic environment, then the PEG-SPIONs were precipitated by ether and dissolved in PBS for further experiments. After that, 2 mg PEG-SPIONs were mixed with 2.50  $\mu$ mol EDC and 6.25  $\mu$ mol sulfo-NHS in 950  $\mu$ L PBS buffer and incubated for 15 min at room temperature. Then 1 mg W20 and/or 0.1 mg XD4 (in 50  $\mu$ L of PBS) was added and the reaction was undergoing overnight at 4 °C. The resultant conjugated-SPIONs were collected by centrifugation at 25000 rpm and kept at 4 °C for future use. The conjugative efficiency for W20 or XD4 was calculated by determining the residual protein amount in the supernatant using BCA assay, which was calculated according to the following equation:

## Thioflavin T fluorescence assay

To determine the effects of W20/XD4-SPIONs and W20-SPIONs on A $\beta$  aggregation, 10  $\mu$ M A $\beta$ 42 was mixed with 100  $\mu$ g/ml or 1000  $\mu$ g/ml of SPIONs and incubated at 37 °C without agitation. When monitoring the aggregation kinetics of A $\beta$ 42, a 10  $\mu$ L aliquot of sample was mixed with 190  $\mu$ L ThT solution (5  $\mu$ M), and the ThT fluorescence intensity was measured using a Tecan Safire2 microplate

reader (Tecan, Switzerland) set to 450 nm/482 nm (excitation/emission). Data were obtained from three independent experiments.

## MTT assay

SH-SY5Y cells (obtained from the cell line resource center of Peking Union Medical College, Chinese Academy of Medical Sciences) were maintained in Dulbecco's modified Eagle's medium (DMEM; Hyclone) with 10% fetal bovine serum (FBS) and 1% penicillin/streptomycin at 37 °C under a 5% CO<sub>2</sub> atmosphere. The cells were seeded in 96-well plates with approximately 10000 cells per 100 μL of medium per well. Plates were then incubated at 37 °C for 24 h to allow cells to attach. The SPIONs with or without 4 μM Aβ<sub>42</sub> oligomers were added to the wells and then incubated for an additional 48 h at 37 °C. Cell viability was determined by adding 20 μL of 5 mg/mL MTT to each well. After 3 h of incubation at 37 °C, the supernatants were replaced with a 150 μL aliquot of DMSO in the dark. The absorbance at 570/630 nm was measured by using a SpectraMax M5 microplate reader (Molecular Devices, Sunnyvale, CA). Data were obtained from three independent experiments.

## Measurements for proinflammatory cytokines

BV-2 cells (obtained from the cell line resource center of Peking Union Medical College, Chinese Academy of Medical Sciences) were maintained in DMEM with 10% FBS and 1% penicillin/streptomycin at 37 °C in 5% CO<sub>2</sub>. The cells were treated with the serial of SPIONs with or without 4 μM Aβ<sub>42</sub> oligomers and incubated for 12 h at 37 °C. Then the cell supernatants were collected and the levels of TNF-α and IL-6 were determined using ELISA kits (Neobioscience technology, Beijing, China) according to the manufacturer's protocols. Briefly, the cell supernatants were added to a 96-well ELISA plate and reacted with the relevant primary antibodies followed by HRP-conjugated secondary antibodies. 3,3',5,5'-Tetramethylbenzidine was used as the substrate. The absorbance of the samples was measured at 450 nm using a SpectraMax M5 microplate reader (Molecular Devices, Sunnyvale, CA). Data were obtained from three independent experiments.

## Western blot analysis

Proteins samples from BV-2 cell lysates pretreated with Aβ and a serial of SPIONs were separated by 12% SDS-PAGE gel (Invitrogen) and transferred onto nitrocellulose membrane (Merck Millipore). After blocking with 5% nonfat milk for 1 h at room temperature, the membrane was probed with anti-iNOS (1:1000), anti-COX2 (1:1000) and anti-GAPDH (1:1000) antibodies respectively, and followed by appropriate HRP-conjugated secondary antibodies. Bands in immunoblots were developed with Super-Signal West Pico Plus Chemiluminescent Substrate kit (Pierce, UB278521), and quantified by densitometry using ImageJ software (NIH).

# Animal treatment

APPswe/PS1dE9 transgenic mice were obtained from the Jackson Laboratory. All mice were given food and water *ad libitum* and maintained in a colony room at  $22 \pm 2^\circ\text{C}$  with  $45\% \pm 10\%$  humidity under a 12:12 h light/dark cycle. Six-month old male AD mice were categorized into five groups: PBS-treated ( $n = 8$ ), SPIONs-treated ( $n = 8$ ), XD4-SPIONs-treated ( $n = 8$ ), W20-SPIONs-treated ( $n = 8$ ) and W20/XD4-SPIONs treated ( $n = 8$ ), and their WT littermates were categorized into three groups: PBS-treated ( $n = 8$ ), SPIONs-treated ( $n = 8$ ) and W20/XD4-SPIONs treated ( $n = 8$ ). The mice were administered with a daily dose of 1 mg nanoparticles in 100  $\mu\text{L}$  PBS (0.01 M, pH 7.4) with 15% mannitol via tail vein for 28 days. After the last administration, the behavioral tests were performed.

## Object recognition test

The object recognition test was performed as previously described with slight modifications[30]. Briefly, in the habituation phase, mice were allowed to freely explore the behavioral open-field arena (50 cm  $\times$  50 cm  $\times$  25 cm white plastic box, empty) individually for 5 min one day before the test was initiated. For the training session (Trial 1), mice were allowed to explore for 5 min in the same box having two identical objects in the upper two corners. For the testing session (Trial 2), after a 24 h retention period, the object in the right corner was replaced with a novel object, and the mice were reintroduced to the box and allowed to explore for 5 min. Time spent exploring and sniffing each object was recorded. The results are

expressed as the discrimination index by calculating: 
$$\frac{\text{Time novel} - \text{Time familiar}}{\text{Time novel} + \text{Time familiar}} * 100 (\%)$$
. The box was cleaned with 70% alcohol between tests to eliminate olfactory cues.

## Y-maze test

The Y-maze test consisted of 2 trials separated by an interval of 1 h. The first trial was 10 min in duration and allowed the mouse to explore only two arms (the start and familiar arms) of the maze, with the third arm (novel arm) blocked. In the second trial, the mouse was put in the same starting arm as in trial 1 with free access to all 3 arms for 5 min. The total time spent and the number of entries in the novel arm were video recorded and analyzed. The arms were cleaned with 70% alcohol between trials to eliminate olfactory cues.

## Morris water maze test

The water maze consisted of a pool (110 cm in diameter) containing opaque water ( $22 \pm 1^\circ\text{C}$ ) and a platform (10 cm in diameter) submerged 1 cm under the water. Hidden platform training was carried out twice per day over five consecutive days, with an inter-trial interval of 3-4 h. Mice were allowed to swim for 60 s to find the platform, on which they were allowed to stay for 10 s. The trial ended when the mouse

located the platform. Mice unable to locate the platform were guided to it. 24 h after the acquisition trial, the mice were tested for memory retention in a probe trial in the absence of the hidden platform. The performance of each mouse was monitored using a video camera (Sony, Tokyo, Japan) mounted over the maze and automatically recorded via a video tracking system.

## Immunohistochemistry

Mice were deeply anaesthetized with avertin (250 mg/kg) and transcardially perfused with ice-cold PBS containing heparin (10 U/mL) before sacrificed. Their brains were immediately removed and divided along the sagittal plane. The left brain hemisphere was fixed in 4% paraformaldehyde at 4 °C overnight and processed for paraffin-embedded sections. Coronal paraffin-embedded serial sections of 5 µm thickness were cut on a Leica CM1850 microtome (Leica Biosystems, Buffalo Grove, IL, USA). For immunohistochemistry analysis, sections were deparaffinized and subjected to antigen retrieval using citrate buffer (0.01M, pH 6.0, 0.05% Tween-20) in a steamer at 95 °C for 20 minutes. The sections were then incubated with 3% H<sub>2</sub>O<sub>2</sub> to quench endogenous peroxidases and washed 3 times with 1×TBS. Thereafter, sections were permeabilized and blocked with 10% normal goat serum in 0.3% Triton X-100 PBST for 1 h at room temperature. Subsequently, the sections were incubated with 6E10 (1:100), anti-Iba-1 (1:100) and anti-GFAP (1:100) antibodies, respectively, followed by corresponding HRP-labeled secondary antibody and visualized with diaminobenzidine (DAB). For synaptophysin and PSD-95 staining, sections were immunostained with anti-synaptophysin (1:100) and anti-PSD95 (1:100) antibodies followed by corresponding secondary antibody conjugated to Alexa Fluor 488 (1:200) or Alexa Fluor 594 (1:200). All images were acquired with an Olympus IX73 inverted microscope with DP80 camera. For immunostaining of 6E10, Iba-1 and GFAP, the positively stained area in at least three sections from cortex and striatum per mouse were analyzed, and three fields for each section were imaged and quantified. For immunostaining of PSD-95 and synaptophysin, immunofluorescence intensities were quantified. All images were processed and analyzed by ImageJ Software (National Institutes of Health, USA).

For microglia engulfment analysis, paraffin-embedded sections of 20 µm thickness were immunostained for Aβ with 4G8 (1:100) and microglia marker with anti-Iba-1 antibody (1:100) followed by corresponding secondary antibody conjugated to Alexa Fluor 594 (1:200) and Alexa Fluor 488 (1:200), respectively. The brain sections were imaged on a Leica TCS SP8 confocal microscope. The Aβ puncta engulfed by the Iba-1-positive microglia were quantified. 8-10 microglia cells were analyzed per mouse.

## Brain lysate preparation

The right brain hemisphere was homogenized in RIPA buffer containing protease inhibitor cocktail (Sigma, P2714-1BTL). The tissues were then centrifuged at 14,000 × g for 30 min at 4 °C, and the supernatant (RIPA-soluble fraction) containing soluble Aβ was collected. The pellets were resuspended in

guanidine buffer (5.0 M guanidine-HCl/50 mM Tris-HCl, pH 8.0) and centrifuged at 14,000 × g for 1 h at 4 °C to obtain supernatants containing insoluble A $\beta$  (guanidine-soluble fraction).

## Measurements for A $\beta$ and proinflammatory cytokines in the brain lysates

The levels of RIPA-soluble A $\beta$  and RIPA-insoluble (guanidine-soluble) A $\beta$  in the brain lysates of mice were quantified by ELISA using A $\beta$ 40 and A $\beta$ 42 immunoassay kits (Immuno-Biological Laboratories). For the proinflammatory cytokine measurements, the levels of TNF- $\alpha$ , IL-1 $\beta$  and IL-6 in the brain lysates of mice were determined using corresponding ELISA kits (Neobioscience Technology) according to the manufacturer's protocols.

## Measurement of GSH, GSSG and ROS

The levels of GSH and GSSG in the brain lysates were assayed by commercial kits (Beyotime, S0053). Total GSH was measured by 5, 5-dithiobis (2-nitrobenzoic) acid (DTNB)-GSSG reductase recycling. GSSG was obtained by determining the absorbance of 5-thio-2-nitrobenzoic acid produced from the reaction of the reduced GSH with DTNB according to the manufacturer's protocols. The reduced GSH was obtained by subtracting GSSG from the total GSH. The absorbance was determined at 412 nm by using an MD-M5 microplate reader.

ROS assay was performed as previously described[31]. Briefly, ROS production was fluorometrically monitored using 2, 7-dichlorofluorescein diacetate (DCFDA) mixed with the brain lysates. The intensity of DCF fluorescence generated from carboxy-DCFDA was proportional to the amount of ROS. The fluorescence was determined using an MD-M5 microplate reader (excitation, 485 nm; emission, 530 nm) and the ROS units were calculated.

## Statistical analysis

Data were analyzed with GraphPad Prism v.8. Statistical significance was assessed using the student's *t*-test, one-way or two-way ANOVA followed by Bonferroni *post hoc* test, as appropriate. Results were expressed as group mean  $\pm$  SEM, and  $P < 0.05$  was considered statistically significant. All samples or animals were included for statistical analysis unless otherwise noted in pre-established criteria.

## Declarations

### Ethics approval and consent to participate

Not applicable.

## Consent for publication

Not applicable.

## Availability of data and materials

All data associated with this study are available in the main text or the supplementary materials.

## Competing interests

The authors declare that they have no competing interests.

## Funding

This work was supported by the grants from the National Natural Science Foundation of China (81971610).

## Authors' contributions

R.-T.L. and X.-L.Y. designed experiment, X.-G.L. and S.L analyzed the data, X.-G.L., X.-L.Y. and R.-T.L. wrote the manuscript. X.-G.L., J.Z. and W.-W.Z performed behavioral experiments. L.Z, D.-Q.L. and Y.-R.H. conducted the immunohistochemistry and biochemistry experiments.

## Acknowledgements

This work was supported by the grants from the National Natural Science Foundation of China (81971610).

## References

1. Mattson MP. Pathways towards and away from Alzheimer's disease. *Nature*. 2004;430:631–9.
2. Graham WV, Bonito-Oliva A, Sakmar TP. Update on Alzheimer's Disease Therapy and Prevention Strategies. *Annu Rev Med*. 2017;68:413–30.
3. Panza F, Lozupone M, Logroscino G, Imbimbo BP. A critical appraisal of amyloid-beta-targeting therapies for Alzheimer disease. *Nat Rev Neurol*. 2019;15:73–88.
4. Lacor PN, Buniel MC, Chang L, Fernandez SJ, Gong Y, Viola KL, Lambert MP, Velasco PT, Bigio EH, Finch CE, et al. Synaptic targeting by Alzheimer's-related amyloid beta oligomers. *J Neurosci*. 2004;24:10191–200.
5. Bateman RJ, Xiong C, Benzinger TL, Fagan AM, Goate A, Fox NC, Marcus DS, Cairns NJ, Xie X, Blazey TM, et al. Clinical and biomarker changes in dominantly inherited Alzheimer's disease. *N Engl J Med*. 2012;367:795–804.
6. Perrin RJ, Fagan AM, Holtzman DM. Multimodal techniques for diagnosis and prognosis of Alzheimer's disease. *Nature*. 2009;461:916–22.

7. Hardy J, Selkoe DJ. **The Amyloid Hypothesis of Alzheimer's Disease: Progress and Problems on the Road to Therapeutics.** *Science* 2002, 297.
8. Villemagne VL, Burnham S, Bourgeat P, Brown B, Ellis KA, Salvado O, Szoeki C, Macaulay SL, Martins R, Maruff P, et al. Amyloid  $\beta$  deposition, neurodegeneration, and cognitive decline in sporadic Alzheimer's disease: a prospective cohort study. *Lancet Neurol.* 2013;12:357–67.
9. Ferreira ST, Lourenco MV, Oliveira MM, De Felice FG. Soluble amyloid-beta oligomers as synaptotoxins leading to cognitive impairment in Alzheimer's disease. *Front Cell Neurosci.* 2015;9:191.
10. Selkoe DJ, Hardy J. The amyloid hypothesis of Alzheimer's disease at 25 years. *EMBO Mol Med.* 2016;8:595–608.
11. Ostrowitzki S, Deptula D, Thurfjell L, Barkhof F, Bohrmann B, Brooks DJ, Klunk WE, Ashford E, Yoo K, Xu ZX, et al. Mechanism of amyloid removal in patients with Alzheimer disease treated with gantenerumab. *Arch Neurol.* 2012;69:198–207.
12. Sperling R, Salloway S, Brooks DJ, Tampieri D, Barakos J, Fox NC, Raskind M, Sabbagh M, Honig LS, Porsteinsson AP, et al. Amyloid-related imaging abnormalities in patients with Alzheimer's disease treated with bapineuzumab: a retrospective analysis. *Lancet Neurol.* 2012;11:241–9.
13. Adolfsson O, Pihlgren M, Toni N, Varisco Y, Buccarello AL, Antonietto K, Lohmann S, Piorkowska K, Gafner V, Atwal JK, et al. An effector-reduced anti-beta-amyloid (A $\beta$ ) antibody with unique abeta binding properties promotes neuroprotection and glial engulfment of A $\beta$ . *J Neurosci.* 2012;32:9677–89.
14. Wang X-p, Zhang J-h, Wang Y-j, Feng Y, Zhang X, Sun X-x, Li J-l, Du X-t, Lambert MP, Yang S-g, et al. Conformation-dependent single-chain variable fragment antibodies specifically recognize beta-amyloid oligomers. *FEBS Lett.* 2009;583:579–84.
15. Zhang X, Sun XX, Xue D, Liu DG, Hu XY, Zhao M, Yang SG, Yang Y, Xia YJ, Wang Y, Liu RT. Conformation-dependent scFv antibodies specifically recognize the oligomers assembled from various amyloids and show colocalization of amyloid fibrils with oligomers in patients with amyloidoses. *Biochim Biophys Acta.* 2011;1814:1703–12.
16. Zhao M, Wang SW, Wang YJ, Zhang R, Li YN, Su YJ, Zhou WW, Yu XL, Liu RT. Pan-amyloid oligomer specific scFv antibody attenuates memory deficits and brain amyloid burden in mice with Alzheimer's disease. *Curr Alzheimer Res.* 2014;11:69–78.
17. Zhang H, Su YJ, Zhou WW, Wang SW, Xu PX, Yu XL, Liu RT. Activated scavenger receptor A promotes glial internalization of abeta. *PLoS One.* 2014;9:e94197.
18. Liu XG, Zhang L, Lu S, Liu DQ, Zhang LX, Yu XL, Liu RT. **Multifunctional superparamagnetic iron oxide nanoparticles conjugated with A $\beta$  oligomer-specific scFv antibody and class A scavenger receptor activator show early diagnostic potentials for Alzheimer's Disease.** *International Journal of Nanomedicine* 2020, 15.
19. Cline EN, Bicca MA, Viola KL, Klein WL. The Amyloid-beta Oligomer Hypothesis: Beginning of the Third Decade. *J Alzheimers Dis.* 2018;64:567–610.

20. Vandenberghe R, Riviere ME, Caputo A, Sovago J, Maguire RP, Farlow M, Marotta G, Sanchez-Valle R, Scheltens P, Ryan JM, Graf A. Active Abeta immunotherapy CAD106 in Alzheimer's disease: A phase 2b study. *Alzheimers Dement (N Y)*. 2017;3:10–22.
21. Pasquier F, Sadowsky C, Holstein A, Leterme Gle P, Peng Y, Jackson N, Fox NC, Ketter N, Liu E, Ryan JM, Team ACCS. Two Phase 2 Multiple Ascending-Dose Studies of Vanutide Cridificar (ACC-001) and QS-21 Adjuvant in Mild-to-Moderate Alzheimer's Disease. *J Alzheimers Dis*. 2016;51:1131–43.
22. Nizami S, Hall-Roberts H, Warriar S, Cowley SA, Di Daniel E. **Microglial inflammation and phagocytosis in Alzheimer's disease: Potential therapeutic targets.** *Br J Pharmacol* 2019.
23. Hansen DV, Hanson JE, Sheng M. Microglia in Alzheimer's disease. *J Cell Biol*. 2018;217:459–72.
24. Husemann J, Loike JD, Anankov R, Febbraio M, Silverstein SC. Scavenger receptors in neurobiology and neuropathology: their role on microglia and other cells of the nervous system. *Glia*. 2002;40:195–205.
25. Bamberger ME, Harris ME, McDonald DR, Husemann J, Landreth GE. A cell surface receptor complex for fibrillar beta-amyloid mediates microglial activation. *J Neurosci*. 2003;23:2665–74.
26. Alarcon R, Fuenzalida C, Santibanez M, von Bernhardi R. Expression of scavenger receptors in glial cells. Comparing the adhesion of astrocytes and microglia from neonatal rats to surface-bound beta-amyloid. *J Biol Chem*. 2005;280:30406–15.
27. Stuart LM, Bell SA, Stewart CR, Silver JM, Richard J, Goss JL, Tseng AA, Zhang A, El Khoury JB, Moore KJ. CD36 signals to the actin cytoskeleton and regulates microglial migration via a p130Cas complex. *J Biol Chem*. 2007;282:27392–401.
28. Reed-Geaghan EG, Savage JC, Hise AG, Landreth GE. CD14 and toll-like receptors 2 and 4 are required for fibrillar A{beta}-stimulated microglial activation. *J Neurosci*. 2009;29:11982–92.
29. Prokop S, Miller KR, Heppner FL. Microglia actions in Alzheimer's disease. *Acta Neuropathol*. 2013;126:461–77.
30. Southwell AL, Warby SC, Carroll JB, Doty CN, Skotte NH, Zhang W, Villanueva EB, Kovalik V, Xie Y, Pouladi MA, et al. A fully humanized transgenic mouse model of Huntington disease. *Hum Mol Genet*. 2013;22:18–34.
31. Zha J, Liu XM, Zhu J, Liu SY, Lu S, Xu PX, Yu XL, Liu RT. A scFv antibody targeting common oligomeric epitope has potential for treating several amyloidoses. *Sci Rep*. 2016;6:36631.

## Figures

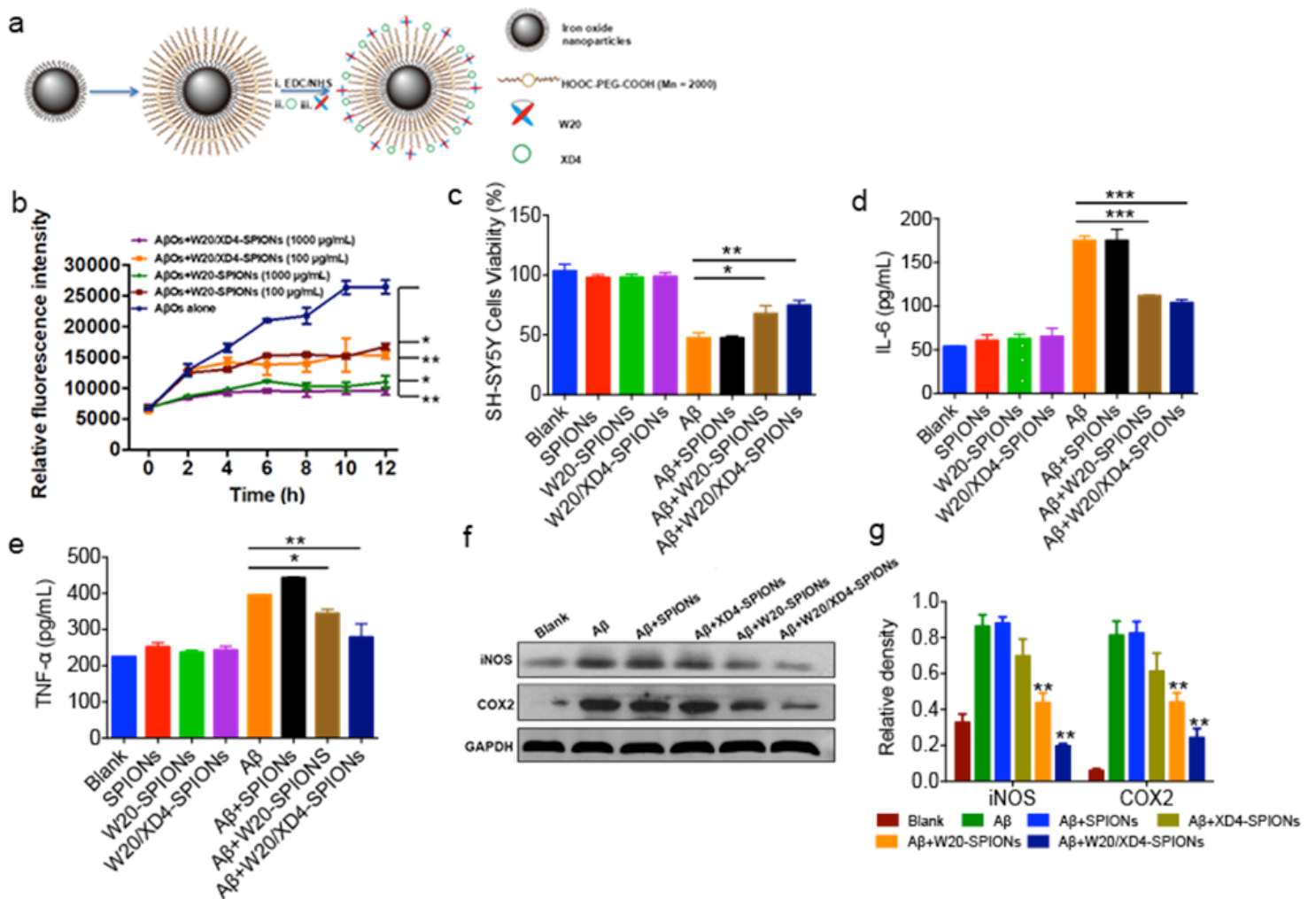


**Figure 1**

W20/XD4-SPIONs inhibited Aβ aggregation and cytotoxicity and reduced inflammatory factor production in vitro. (a) Schematic illustration of preparation of W20/XD4-SPIONs. i: The carboxyl of PEG on the SPIONs were activated with EDC and NHS. SR-A activator XD4 (ii) and oligomer-specific scFv antibody W20 (iii) were conjugated to the nanoparticles. (b) The aggregation kinetics of Aβ incubated with or without 100 or 1000 µg/mL W20-SPIONs or W20/XD4-SPIONs was assessed by thioflavin T fluorescence assay. (c) SH-SY5Y cells were treated with unconjugated-SPIONs, W20-SPIONs or W20/XD4-SPIONs in the presence or absence of 4 µM AβOs for 72 h, the cell viability was determined by MTT assay. (d-e) The levels of IL-6 (d) and TNF-α (e) in the supernatants of BV-2 cells treated with unconjugated-SPIONs, W20-SPIONs or W20/XD4-SPIONs in the presence or absence of 1 µM AβOs were determined using corresponding ELISA kits. (f) Western-blot analysis of iNOS and COX2 in the BV-2 cell lysates treated with unconjugated-SPIONs, W20-SPIONs, XD4-SPIONs or W20/XD4-SPIONs in the presence of 1 µM AβOs or AβOs alone. (g) Quantification of iNOS and COX2 in (f). Data represent means ± SEM. \*P < 0.05, \*\*P < 0.01, \*\*\*P < 0.001.

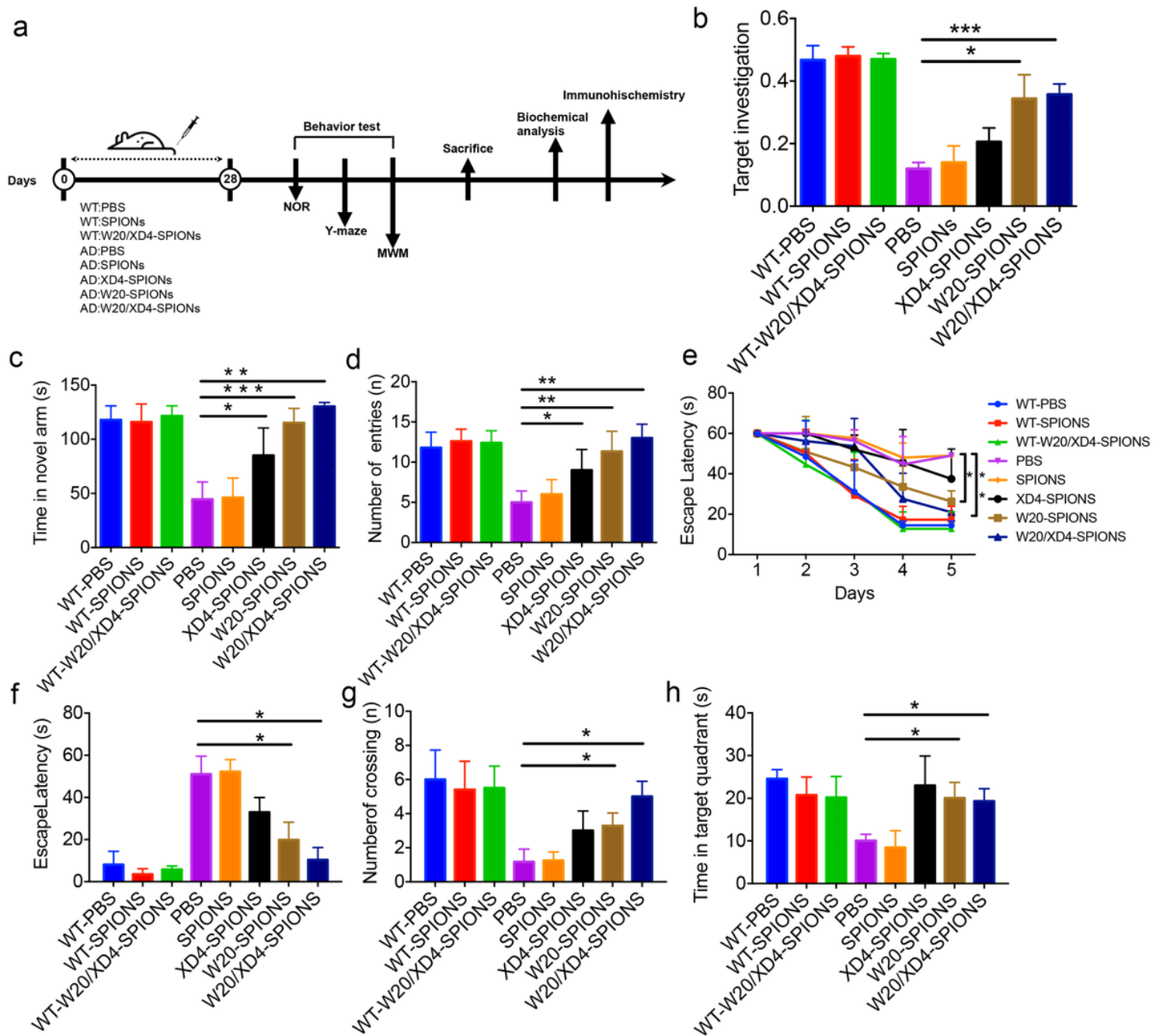


**Figure 2**

W20/XD4-SPIONs rescued cognitive deficits in AD mice. (a) Schematic representation of pharmacological treatment and experimental measurement. (b) The object recognition test was performed on AD mice and their WT littermates treated with various SPIONs. The results were expressed as discrimination index. (c and d) The short-term memory of AD mice and their WT littermates treated with various SPIONs was measured by Y-maze. The time spent in the novel arm (c) and the number of entries (d) were recorded. (e-h) Spatial learning and memory retention of AD mice and their WT littermates treated with various SPIONs were assessed using the Morris water maze. (e) During training trials, the latency to find the hidden platform was measured. (f-h) During probe trials, the latency to the position of

the removed platform (f), the number of platform crossings (g) and the time spent in target quadrant (h) were determined. n = 8 mice/group. Data represent means  $\pm$  SEM. \*P < 0.05, \*\*P < 0.01, \*\*\*P < 0.001.

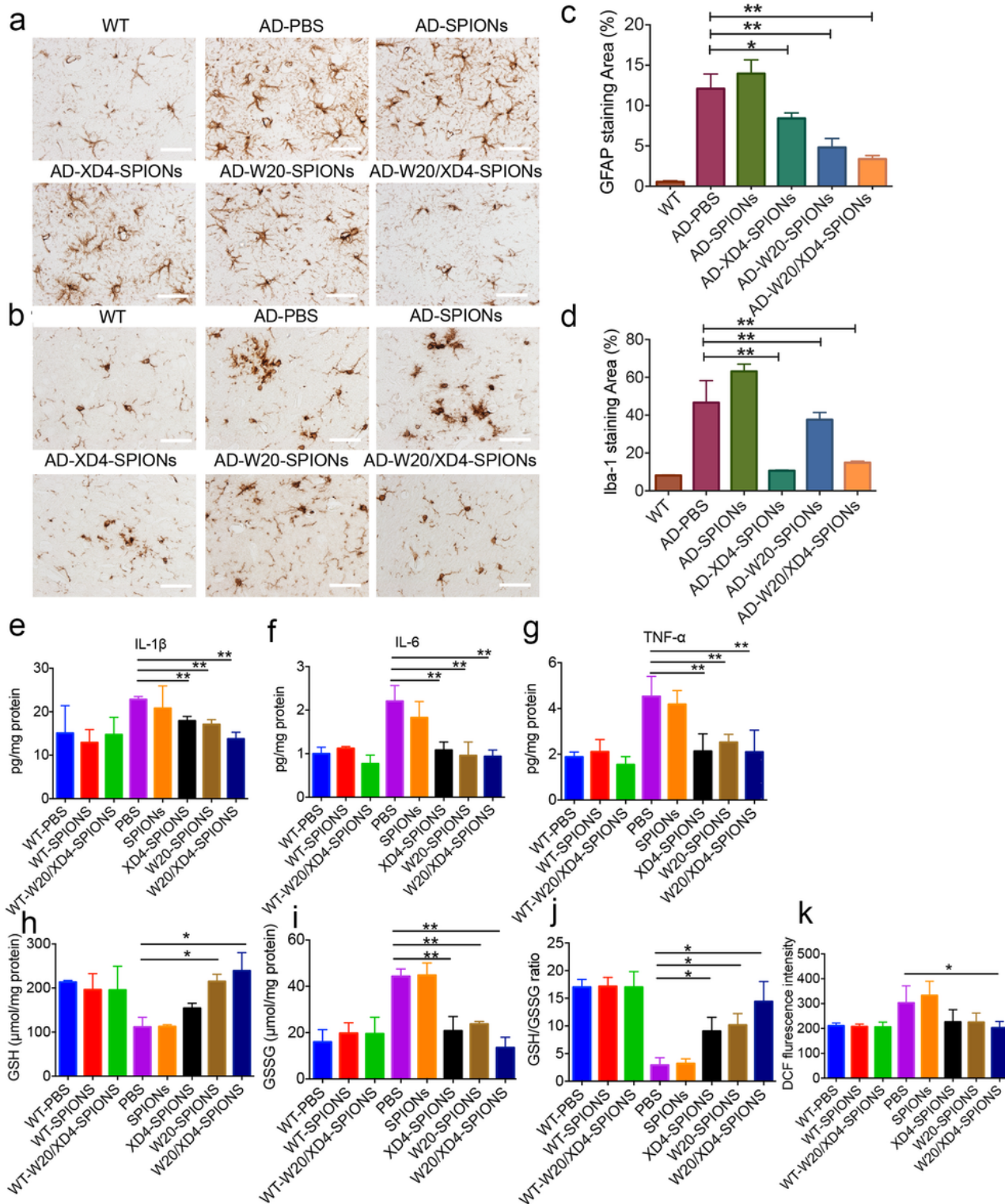


**Figure 3**

W20/XD4-SPIONs reduced oxidative stress and neuroinflammation in the brains of AD mice. (a-b) GFAP immunostaining (a) and Iba-1 immunostaining (b) in the brains of AD mice treated with various SPIONs. Scale bar, 250  $\mu$ m. (c-d) Quantification of GFAP (c) and Iba-1 (d) immunostaining. (e-g) The levels of IL-1 $\beta$

(e), IL-6 (f), and TNF- $\alpha$  (g) in the brain lysates of AD mice and their WT littermates treated with various SPIONs were determined using corresponding ELISA kits. (h-k) The levels of GSH (h), GSSG (i), GSH/GSSG ratio (j) and ROS (k) in the brain lysates of AD mice and their WT littermates treated with various SPIONs were determined using corresponding commercial kits. n = 8 mice/group. Data represent means  $\pm$  SEM. \*P < 0.05, \*\*P < 0.01.

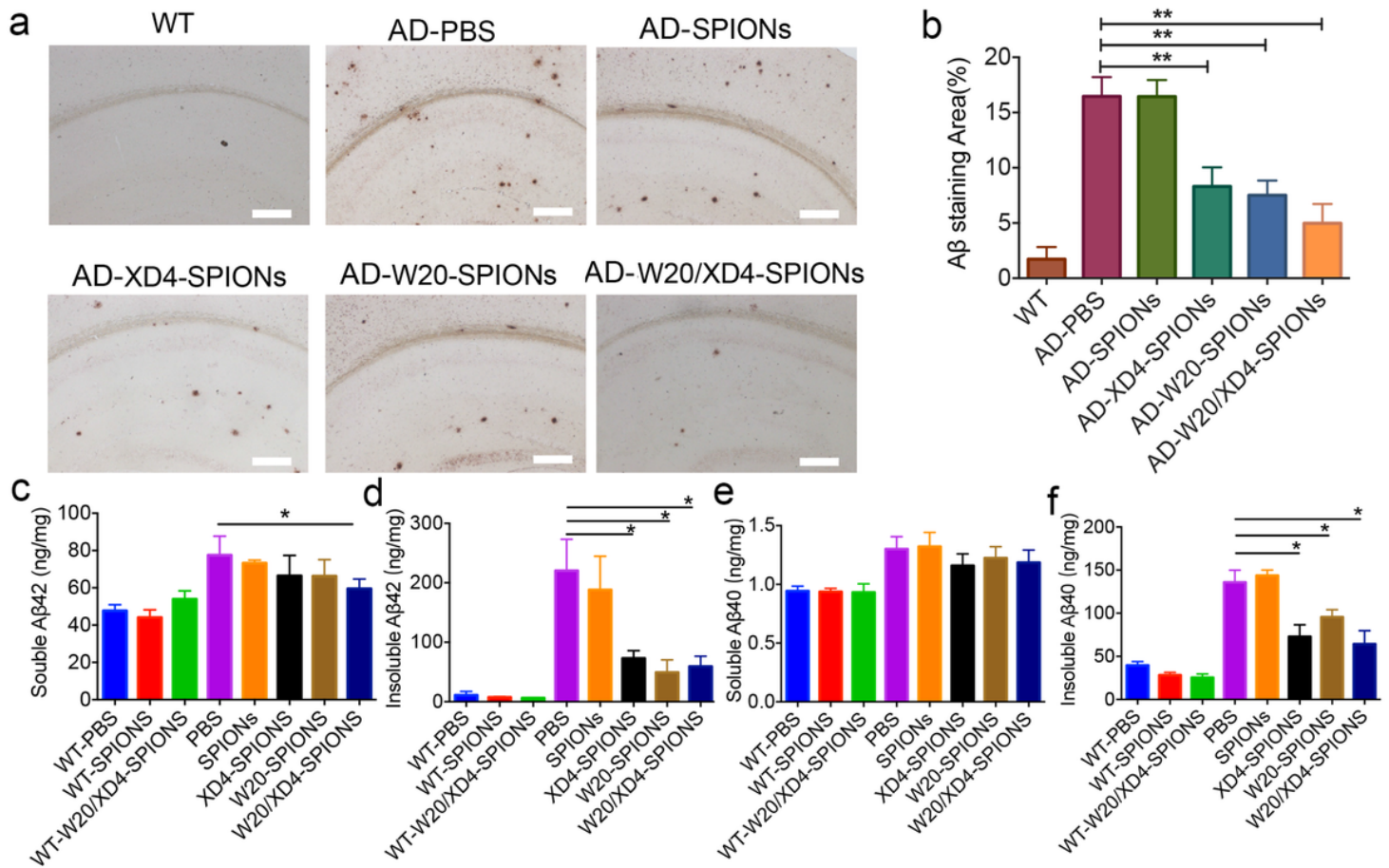


**Figure 4**

W20/XD4-SPIONs attenuated A $\beta$  pathology in the brains of AD mice. (a) 6E10 immunostaining for plaques in the brains of WT and AD mice treated with various SPIONs. Scale bars: 400  $\mu$ m. (b) Quantification of A $\beta$ -immunostaining areas in (a). (c-f) The levels of soluble A $\beta$ 42 (c), insoluble A $\beta$ 42 (d), soluble A $\beta$ 40 (e) and insoluble A $\beta$ 40 (f) in the brain lysates of AD mice and their WT littermates treated with various SPIONs were detected by ELISA. n = 8 mice/group. Data represent means  $\pm$  SEM. \*P < 0.05, \*\*P < 0.01.

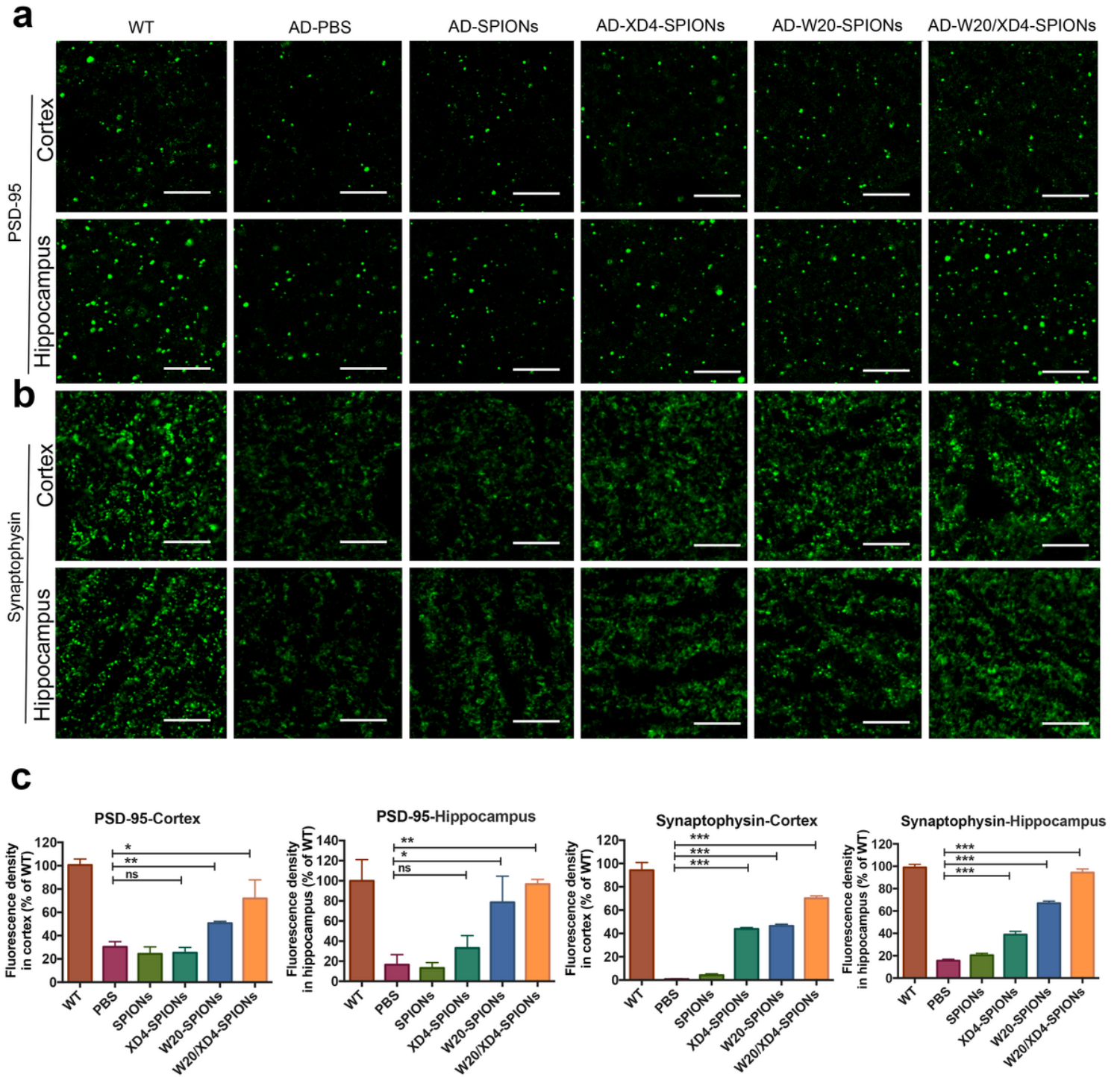


**Figure 5**

W20/XD4-SPIONs rescued synapse loss in the brains of AD mice. (a and b) The PSD-95 immunostaining (a) and synaptophysin immunostaining (b) in the brains of WT and AD mice treated with various SPIONs. Scale bar, 10  $\mu$ m. (c) Quantification of PSD-95 and synaptophysin immunostaining in the cortex and hippocampal regions. n = 8 mice/group. Data represent means  $\pm$  SEM. \*P < 0.05, \*\*P < 0.01, \*\*\*P < 0.001.

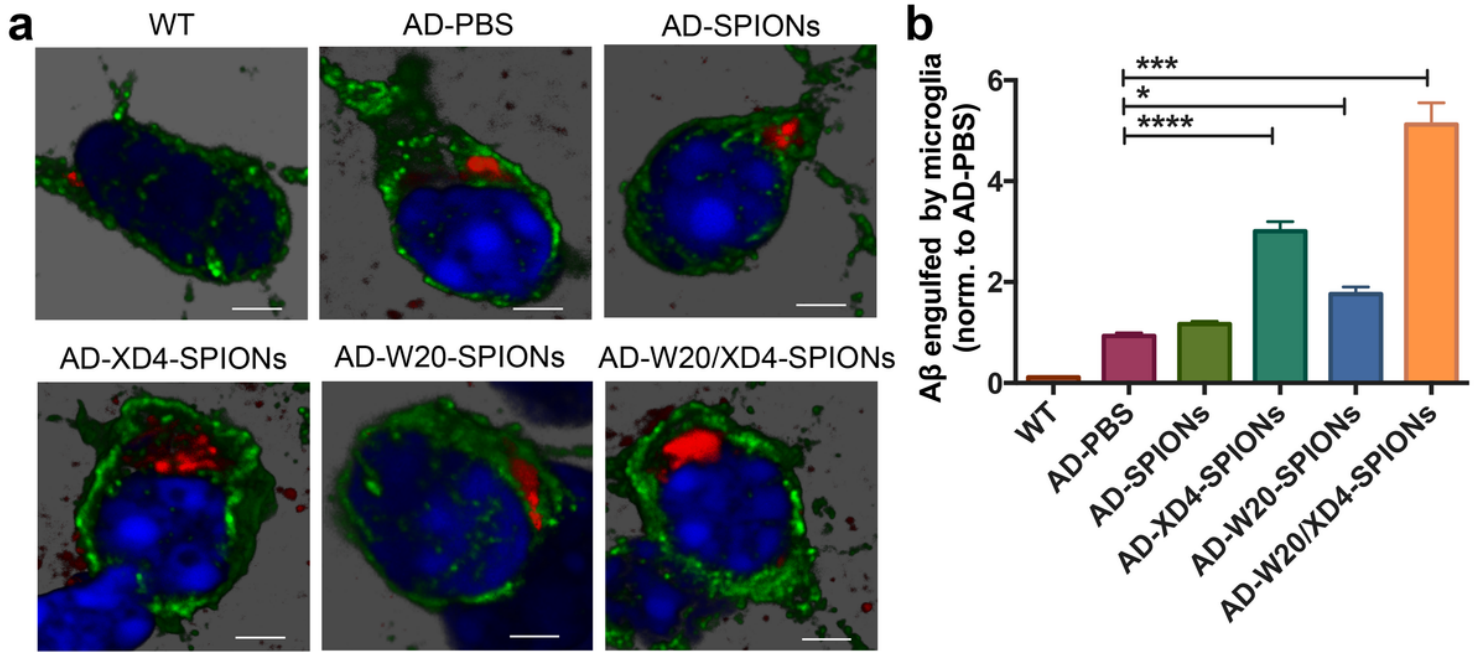


**Figure 6**

W20/XD4-SPIONs promoted microglial engulfment of A $\beta$  in AD mice. (a) Representative images of Iba-1 positive microglia (green) and engulfed A $\beta$  puncta (red) in WT and AD mice treated with various SPIONs. (b) Quantification of A $\beta$  puncta engulfed in Iba-1 positive microglia, normalized to PBS-treated AD controls. Scale bars, 500 nm. Data represent means  $\pm$  SEM. \*P < 0.05, \*\*\*P < 0.001, \*\*\*\*P < 0.0001.